Research Article | Vol. 26, No. 6 | 19 Mar 2018 | OPTICS EXPRESS 7056
Optics EXPRESS

Robust, tunable, and high purity triggered single photon source at room temperature using a nitrogen-vacancy defect in diamond in an open microcavity

P. R. Dolan,[1] S. Adekanye,[1] A. A. P. Trichet,[1] S. Johnson,[1] L. C. Flatten,[1] Y. C. Chen,[1] L. Weng,[1], D. Hunger,[2] H.-C. Chang,[3] S. Castelletto,[4] and J. M. Smith.[1*]

[1]*Department of Materials, University of Oxford, Parks Road, Oxford OX1 3PH, UK*
[2]*Fakultät für Physik, Ludwig-Maximilians-Universität, Schellingstraße 4, 80799 München, Germany*
[3]*Institute of Atomic and Molecular Sciences, Academia Sinica, Taipei 106, Taiwan*
[4]*School of Engineering, RMIT University, Melbourne, Victoria 3001, Australia*
[*]*jason.smith@materials.ox.ac.uk*

Abstract: We report progress in the development of tunable room temperature triggered single photon sources based on single nitrogen-vacancy (NV) centres in nanodiamond coupled to open access optical micro-cavities. The feeding of fluorescence from an NV centre into the cavity mode increases the spectral density of the emission and results in an output stream of triggered single photons with spectral line width of order 1 nm, tunable in the range 640 - 700 nm. We record single photon purities exceeding 96% and estimated device efficiencies up to 3%. We compare performance using plano-concave microcavities with radii of curvature from 25 μm to 4 μm and show that up to 17% of the total emission is fed into the TEM_{00} mode. Pulsed Hanbury-Brown Twiss (HBT) interferometry shows that an improvement in single photon purity is facilitated due to the increased spectral density.

OCIS codes: (230.0230) Optical devices; (270.0270) Quantum optics.

References and links

1. X. Brokmann, G. Messin, P. Desbiolles, E. Giacobino, M. Dahan, and J. P. Hermier , "Colloidal CdSe/ZnS quantum dots as single-photon sources," New J. Phys. **6**, 99 (2004).
2. L. Li, E. H. Chen, J. Zheng, S. L. Mouradian, F. Dolde, T. Schröder, S. Karaveli, M. L. Markham, D. J. Twitchen, and D. Englund, "Efficient photon collection from a nitrogen vacancy center in a circular bullseye grating," Nano Lett. **15**(3), 1493 (2015).
3. T. T. Tran, K. Bray, M. J. Ford, M. Toth, and I. Aharonovich, "Quantum emission from hexagonal boron nitride monolayers," Nature Nanotech. **11**(1), 37 (2011).
4. A. K. Nowak, S. L. Portalupi, V. Giesz, O. Gazzano, C. Dal Savio, P.-F. Braun, K. Karrai, C. Arnold, L. Lanco, I. Sagnes, A. Lemaître and P. Senellart, "Deterministic and electrically tunable bright single-photon source," Nature Commun. **5**, 3240 (2014).
5. C. Kurtsiefer, S. Mayer, P. Zarda, and H. Weinfurter, "Stable solid-state source of single photons," Phys. Rev. Lett. **85**(2), 290 (2000).
6. Quantum Cryptography Victoria - http://qcvictoria.com/
7. K. J. Vahala, "Optical microcavities," Nature **424**(6950), 839–846 (2003).
8. A. Auffèves, J.-M. Gérard, and J.-P. Poizat, "Pure emitter dephasing: A resource for advanced solid-state single-photon sources," Phys. Rev. A **79**, 053838 (2009).
9. Y. Dumeige, Romain Alléaume, Philippe Grangier, François Treussart and Jean-François Roch, "Controlling the single-diamond nitrogen-vacancy color center photoluminescence spectrum with a Fabry-Pérot microcavity," New J. Phys. **13**, 025015 (2011).
10. M. Trupke, E. A. Hinds, S. Eriksson, E. A. Curtis, Z. Moktadir, E. Kukharenka, and M. Kraft, "Microfabricated high-finesse optical cavity with open access and small volume," Appl. Phys. Lett. **87**, 211106 (2005).
11. G. Cui, J. M. Hannigan, R. Loeckenhoff, F. M. Matinaga, M. G. Raymer, S. Bhongale, M. Holland, S. Mosor, S. Chatterjee, H. M. Gibbs, and G. Khitrova, "A hemispherical, high-solid-angle optical micro-cavity for cavity-QED

#309805 https://doi.org/10.1364/OE.26.007056
Journal © 2018 Received 23 Oct 2017; revised 4 Jan 2018; accepted 4 Jan 2018; published 8 Mar 2018

Optics EXPRESS

studies," Opt. Express **14**(6), 2289 (2006).
12. T. Steinmetz, Y. Colombe, D. Hunger, T. W. Hänsch, A. Balocchi, R. J. Warburton, and J. Reichel, "Stable fiber-based Fabry-Pérot cavity," Appl. Phys. Lett. **89**, 111110 (2006).
13. P. R. Dolan, G. M. Hughes, F. Grazioso, B. R. Patton, and J. M. Smith, "Femtoliter tunable optical cavity arrays," Opt. Lett. **35**(21), 3556 (2010).
14. D. Hunger, T. Steinmetz, Y. Colombe, C. Deutsch, T. W. Hänsch, and J. Reichel, "A fiber Fabry-Perot cavity with high finesse," New J. Phys. **12**, 065038 (2010).
15. R. J. Barbour, P. A. Dalgarno, A. Curran, K. M. Nowak, H. J. Baker, D. R. Hall, N. G. Stoltz, P. M. Petroff, and R. J. Warburton, "A tunable microcavity," J. Appl. Phys. **110**(5), 053107 (2011).
16. D. Hunger, C. Deutsch, R. J. Barbour, R. J. Warburton, J. and Reichel, "Laser micro-fabrication of concave, low-roughness features in silica," AIP Advances **2**, 012119 (2012).
17. Z. Di, H. V. Jones, P. R. Dolan, S. M. Fairclough, M. B. Wincott, J. Fill, G. M. Hughes, and J. M. Smith, "Controlling the emission from semiconductor quantum dots using ultra-small tunable optical microcavities," New J. Phys. **14**(10), 103048 (2012).
18. H. Kaupp, C. Deutsch, H. C Chang, J. Reichel, T. W. Hänsch, and D. Hunger, "Scaling laws of the cavity enhancement for nitrogen-vacancy centers in diamond," Phys. Rev. A **88**, 053812 (2013).
19. R. Albrecht, A. Bommer, C. Deutsch, J. Reichel, and C. Becher, "Coupling of a single NV-center in diamond to a fiber-based microcavity," Phys. Rev. Lett. **110**, 243602 (2013).
20. R. Albrecht, A. Bommer, C. Pauly, F. Mücklich, A. W. Schell, P. Engel, T. Schröder, O. Benson, J. Reichel, and C. Becher, "Narrow-band single photon emission at room temperature based on a single nitrogen-vacancy center coupled to an all-fiber-cavity," Appl. Phys. Lett. **105**, 073113 (2014).
21. S. Johnson, P. R. Dolan, T. Grange, A. A. P. Trichet, G. Hornecker, Y. C. Chen, L. Weng, G. M. Hughes, A. A. R. Watt, A. Auffèves and J. M. Smith, "Tunable cavity coupling of the zero phonon line of a nitrogen-vacancy defect in diamond," New J. Phys. **17**, 122003 (2015).
22. D. Riedel, I. Söllner, B. J. Shields, S. Starosielec, P. Appel, E. Neu, P. Maletinsky, and R. J. Warburton, "Deterministic enhancement of coherent photon generation from a nitrogen-vacancy center in ultrapure diamond," Phys. Rev. X **7**, 031040 (2017)
23. H. Kaupp, T. Hümmer, M. Mader, B. Schlederer, J. Benedikter, P. Haeusser, H.C.Chang, H. Fedder, T. W. Hänsch, D. Hunger, "Purcell-enhanced single-photon emission from nitrogen-vacancy centers coupled to a tunable microcavity," Phys. Rev. Appl. **6**, 054010 (2016).
24. J. Benedikter, H. Kaupp, T. Hümmer, Y. Liang, A. Bommer, C. Becher, A. Krueger, J. M. Smith, T. W. Hänsch, and D. Hunger, "Cavity-enhanced single-photon source based on the silicon-vacancy center in diamond," Phys. Rev. Appl. **7**, 024031 (2017).
25. D. Wang, H. Kelkar, D. Martin-Cano, T. Utikal, S. Götzinger, and V. Sandoghdar, "Coherent coupling of a single molecule to a scanning Fabry-Pérot microcavity," Phys. Rev. X **7**, 021014 (2017).
26. S. Schietinger, M. Barth, T. Aichele, and O. Benson, "Plasmon-enhanced single photon emission from a nanoassembled metal-diamond hybrid structure at room temperature," Nano Lett. **9**, 1694 (2009).
27. A. A. P. Trichet, P. R. Dolan, D. M. Coles, G. M. Hughes, and J. M. Smith, "Topographic control of open-access microcavities at the nanometer scale," Opt. Express **23**(13), 17205 (2015).

1. Introduction

The realisation of a convenient triggered single photon source (SPS) device that operates at ambient temperature remains an outstanding challenge in the field of photonics. Such a device would be an important enabling technology for quantum science and technology in general, with prospects for use in quantum cryptography, metrology and sensing. Many single quantum systems have been shown to exhibit non-classical photon emission characteristics [1–4], but most suffer fundamental limitations such as instability, or require low temperature operation. Whilst tremendous progress has been made in recent years with the engineering of high quality single photon sources based on semiconductor quantum dots operating at cryogenic temperatures, the first commercial devices of this type will inevitably be quite bulky and costly to manufacture, and so devices with the potential to deliver robust, room temperature sources remain of considerable interest.

Of the available candidate systems for a room temperature SPS, Nitrogen-vacancy (NV) centres in diamond have been shown to be both bright and stable [5], with single photon emission robust to extended optical pumping, modest thermal cycling and exposure to an oxidising atmosphere. NV centres in nanodiamond have been used in a previous commercial single photon source device [6], but the spectrally broad emission from an NV centre emitting into free space or a bulk

Optics EXPRESS

material (full-width at half-maximum of about 60 nm between 650 nm and 710 nm) is not well suited to most applications. Optical microcavities [7] provide a practical solution to this problem. Coupling of spectrally broad emission to a narrow microcavity mode - the so-called 'bad emitter regime' of cavity quantum electrodynamics - results in the 'feeding' of emitted photons into the cavity mode [8] such that the emission takes on the spectral and spatial properties of the mode without substantial loss of intensity [9]. Since microcavity modes can be engineered to have desirable spatial properties for coupling into external optics and can be tuned spectrally, the emission can also be tailored for practical device applications. In particular the increased spectral density achieved by the feeding process is of benefit for low light level free-space applications where the emitted photons must be distinguished from a broad ambient background. The relatively broad band emission of the NV centre also offers the attraction of a wide spectral tuning range with potential for wavelength division multiplexing of single photon streams.

To maximise the efficiency of a room temperature NV-cavity device it is essential to minimise the cavity mode volume as far as is possible, and with this in mind, cavity coupling using plasmonic structures [26], and ultra small Fabry Pérot cavities with metal mirrors [23] have been demonstrated. These approaches can lead to high out-coupling efficiency but offer little ability to control or tune the spectra, and single photon fidelity can be compromised by autofluorescence from the metal components.

Here we report the performance of room temperature devices in which single NV centres in nanodiamond are coupled to open microcavities consisting one planar and one concave mirror. This particular style of microcavity has become increasingly popular in recent years for their ease of alignment, tunability, and efficient coupling to external optics [10–16]. A wide range of experiments coupling single photon emitters to open cavities has been reported, including quantum dots [17], diamond colour centres [18–24], and single molecules [25]. Much of the preceding work has been concerned with coupling NV centres to cavities with relatively high quality factors [18–21], or with metallic mirrors and much lower cavity quality factors [23]. In the experiments reported here we use dielectric mirrors to produce open microcavities with intermediate finesse, providing a combination of narrow spectral line width, high single photon fidelity, high spectral density, tunability and modest device efficiencies. We use focused ion beam (FIB) milling to achieve precise fabrication of the concave mirror template with radius of curvature (RoC) between 4 μm and 25 μm, thus allowing systematic comparison of performance as a function of microcavity design. We find that best performance is achieved with RoC = 8 μm, providing a balance between strongest cavity feeding and efficient photon extraction from the cavity mode into the external optics. Specifications of these single photon sources are characterised in detail.

2. Method

The nanodiamonds (NDs) used in this work were commercially available high-pressure high-temperature material (Microdiamant) between 35 nm and 100 nm in diameter, which had been cleaned using a tri-acid mixture and centrifuged to narrow the size distribution. Plano-concave open access microcavities were formed between two decoupled substrates; one planar mirror and one featured mirror (inset, figure 1(d)). Production of the featured mirror begins with a 500 μm thick fused silica substrate (UQG Optics). A silicon dicing saw is used to score trenches ~200 μm deep across most of the surface, leaving small protruding plinths $\sim 300 \times 300$ μm in size (figure 1(a)) as reaching cavity lengths ~ 1 μm is problematic using substrates with larger surface areas. Concave features 600 nm in depth are formed on the plinth using a FIB [13, 27] and the substrate is then commercially coated (LaserOptik) with 16 pairs of Distributed Bragg Reflector (DBR) layers yielding a peak reflectivity $R_f > 99.99\%$ at 640 nm, and a transmission of $\sim 50\%$ at 532 nm. The ion beam sputtered dielectric layers consist of silica (SiO_2 $n_r = 1.49$) and tantalum pentoxide (Ta_2O_5 $n_r = 2.1$) for a high refractive index contrast as well as a high packing density

Optics EXPRESS

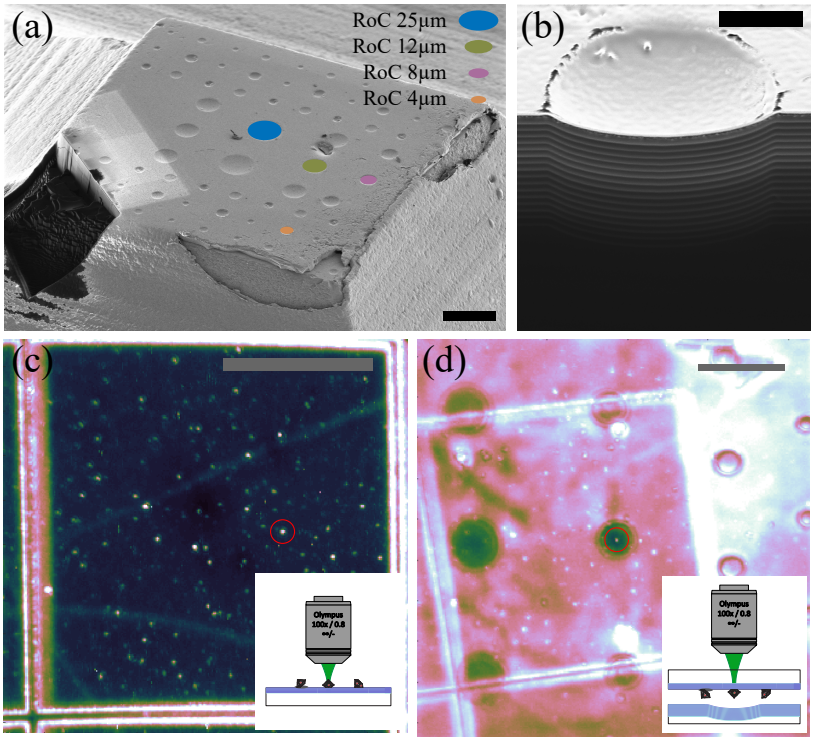

Fig. 1. (a) A scanning electron micrograph (SEM) of a fused silica plinth with multiple RoC features FIB milled onto surface and then deposited with DBR coating. A sputtered gold coating has been applied to facilitate electron imaging. Feature RoCs are highlighted and the scale bar is 20 μm (b) Cross sectional SEM of an RoC 8 μm feature showing the deposited DBR layers where the scale bar is 5 μm.(c) A photoluminescence (PL) image showing NV fluorescence when DBR oriented to face the objective lens. NV1 is circled in red and the scale bar is 20 μm.(d) PL image of the same region inverted and arranged in front of an array of optical microcavities. NV1 is circled in red and the scale bar is 20 μm. Insets show sketches of sample arrangements.

to minimise absorptive and scattering losses within the DBR. The featured mirror is terminated with Ta_2O_5 to minimise mode penetration into the mirror as well as minimising the contribution of surface contaminants to intra-cavity scattering due to a node of the resonant field forming at the substrate surface. The planar substrate is coated with 11 pairs of layers to act as the out-coupler of the resonator ($R_p \sim 99.7\%$), and is terminated with a SiO_2 layer to ensure an antinode of the electric field at the mirror surface for strong interaction with the spin-cast nanodiamond. The planar mirrors were marked with a Ga^+ FIB (FEI FIB200) prior to spin-coating with the ND suspension, to provide a reference 'grid' that allow specific NDs to be located when the mirror is inverted.

Characterisation of the NDs and measurement of the device performance was carried out using a home-built scanning confocal microscope based on a steering mirror (Newport FSM 300-01) directing a 532 nm excitation source (Oxxius LCX-532L, 250 mW) through a 4-f telecentric lens pair to an Olympus 0.8 N.A air objective lens. For pulsed excitation an amplified picosecond pulsed laser diode at 531 nm (Picoquant LDH-P-FA-530B) was used. Collected fluorescence was passed through a 50 μm pin hole followed by a free space 50:50 beam splitter with one output directed onto a single photon avalanche diode (SPAD, Excelitas SPCM-AQRH-14-TR) and the other to a multi-mode fibre which could be coupled to either a fibre-coupled SPAD, or a

Optics EXPRESS

spectrometer.

To identify suitable single NV centres for cavity coupling, fluorescence from the spin-cast nanodiamonds on the planar mirror is first imaged as shown in figure 1(c). Peaks in intensity are identified by an image processing script and an automatic sequence conducts Hanbury Brown and Twiss (HBT) interferometry on each. This was found to be an effective way to both photo-bleach unstable features, and allow the remaining peaks to be rapidly assayed to identify strong and stable single photon emitters. The fluorescence saturation intensity and saturation excitation power (I_{sat} & P_{sat} respectively) were measured for each of these selected NV centres, and the orientation of their axis of symmetry found by rotating the excitation polarisation. The polarisation state of the emitted photons was not investigated during this study however the TEM_{00} for the cavities used here is degenerate for orthogonal polarisation states, and so the polarisation properties of the NV centre's emission are thought to be unaffected by its coupling to these cavity modes. The fluorescence spectrum was recorded to ensure that the NV centre remained predominantly in the negative charge state. Time-correlated single photon counting yields the excited state lifetime through time-resolved photoluminescence (TRPL), and HBT measurements were performed with pulsed excitation to establish the single photon emission fidelity.

Once the selected NVs have been fully characterised, the planar mirror is inverted and the same NV centres relocated using the registration marks, allowing a concave mirror to be positioned behind a chosen NV as shown in figure 1(d). The cavity coupling and tuning is then achieved by reducing the cavity length with a piezoelectric actuator. The plano-concave resonators display Hermite-Gauss mode structure, denoted by TEM_{nm}, where n and m are the orders of the Hermite polynomials describing the field distribution in the x and y directions respectively.

3. Results and analysis

Figure 2 shows fluorescence spectra and images obtained from coupling the same NV centre (NV1) to cavities with concave mirror RoCs 25, 12, 8 and 4 μm and diameters 10, 7.5, 5.5 and 4 μm respectively. Coupling of the NV emission to multiple cavity modes is observed in each of the spectra in figure 2(a), with the strong, regularly spaced modes corresponding to the transverse excitations of the primary TEM_{00} modes. In each case the cavity length was minimised such that only a few field nodes existed between the mirror surfaces. Careful positioning of the NV centre on the axis of the cavity results in optimal coupling to the modes with m,n both even and negligible coupling to modes with odd m or n. In figure 2(a) such optimal alignment is apparent from the RoC 25 and 12 μm cavities whereas for the two smallest cavities some coupling to odd modes is also observed. The TEM_{00} mode was found to dominate the measured output increasingly as the RoC was reduced. This observation is explained by the larger numerical apertures of the higher transverse modes in the smaller RoC cavities, such that these modes have higher clipping losses at the edges of the concave mirrors and couple less efficiently into the microscope objective.

As well as modulating the output spectrum, closing the cavity increases the device efficiency. Figure 3(a) shows the effect of the cavity length on the detected photon count rate from a single NV centre coupled to a RoC 8 μm cavity. As the cavity length is reduced, oscillation in the measured intensity is observed as the modes of successive longitudinal index pass through resonance with the NV emission. The inset for figure 3(a) highlights the first maximum, and indicates approximate locations corresponding to the observed spectra in figure 3(b). A strong device output signal persists over a 40 nm spectral range. In the uppermost spectrum of figure 3(b) the next higher family of TEM_{mn} modes, allows for the free spectral range (FSR) to be ascertained. A 1D transfer matrix approach was used to model this transmission spectrum, revealing that it corresponds to a physical mirror separation of 980 nm. The mode penetration into the mirrors can also be included by taking the value at which the field intensity drops to $1/e$ of its intra cavity value, yielding a total optical path length of L = 1.77 μm. Lateral mode

Optics EXPRESS

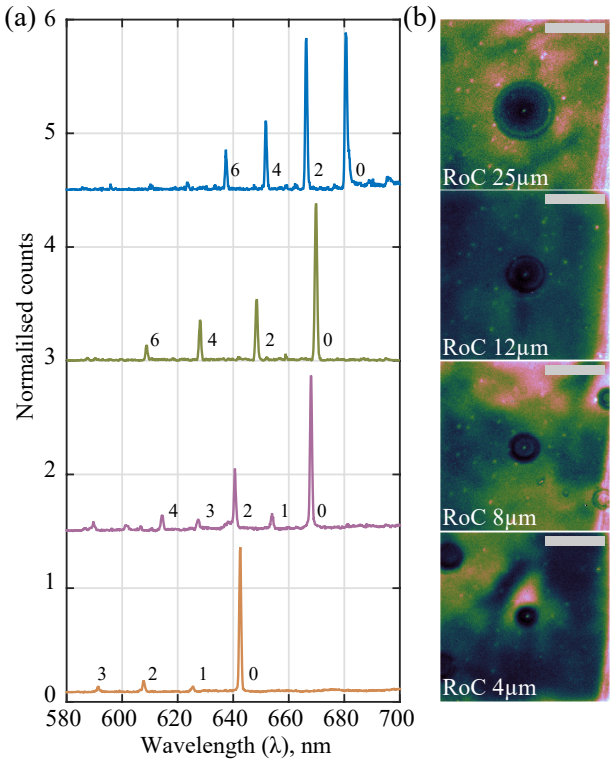

Fig. 2. (a) Spectra collected from a single NV centre (NV1) coupled to open access microcavities with radii of curvature 25, 12, 8 and 4 μm from top to bottom. Peaks are labelled according to the sum of their Hermite-Gauss trnasverse mode indices. (b) PL images of NV1 coupled to the four cavities. The scale bar is 15 μm.

spacings were calculated using resonator theory, and also by importing AFM topographies into FDTD simulations. Both approaches show the transverse mode spacings to be in excellent agreement with the experimentally recorded data. Calculating the cavity finesse from the FSR and homogeneous linewidth yields $\mathcal{F} = \frac{\Delta\lambda}{\delta\lambda} = 270$, which is an order of magnitude lower than the value suggested by only considering the average reflectivity of the mirrors (~ 2200). This implies the other sources of loss which is probably a combination of those associated with the contoured DBR in the mirror feature seen previously [13] and scattering from the ND itself and other surface contaminants.

Figure 3(c) shows the spectrum of NV2 observed whilst the DBR was facing towards the objective lens (blue data) with a peak emission intensity at a wavelength of around 660 nm. This peak wavelength is slightly blue-shifted compared with the free-space emission of the NV centre due to the reflection band of the dielectric mirror. Using FDTD simulations to simulate the effect of the mirror on collected fluorescence, we reconstruct the free-space NV emission spectrum (green data) which peaks at a wavelength of 680 nm. This spectrum agrees well with the relative intensities of the TEM_{00} modes recorded as the cavity is tuned.

The mode coupling efficiency is established by recording the fluorescence intensity as a function of excitation power and fitting with the function $N = \frac{PN_{sat}}{P_{sat}+P} + BP$. Here N is the measured fluorescence count rate on the SPAD and P is the laser power at the objective back aperture, while the saturation count rate N_{sat}, the saturation power, P_{sat} and the background contribution B are fitting parameters. A power dependence is first recorded from the DBR without

Optics EXPRESS

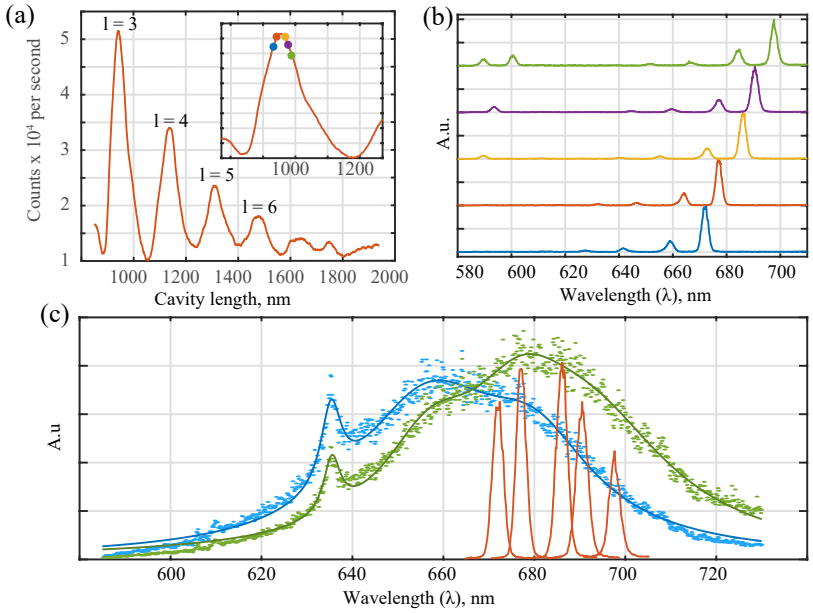

Fig. 3. (a) Enhanced photon count rates for a RoC 8 μm feature closed around NV2. Peak labels show the number of field antinodes between the mirrors. The inset shows the approximate cavity lengths of spectra shown in (b). (b) Collected spectra at several points observed by tuning the cavity length over the intensity maximum in a). Note that the line widths shown here are inhomogeneously broadened by spectral drift over the integration time. (c) Observed emission spectrum of NV2 prior to cavity coupling (blue), and inferred emission spectrum of NV2 after removing the effect of the DBR mirror using FDTD (green). TEM_{00} modes (red), show agreement in phonon sideband maximum and optimum fluorescence collection rates.

an NV present. This region was photo-bleached until stable, and is used to provide an initial value for B when fitting the NV's emission. The final fitted background component is subtracted from both the fits and the plotted data for clarity. Here three cases are considered; first the initial NV fluorescence collected with the DBR facing the objective lens (blue), the full NV-cavity coupled emission spectrum (red), and a single TEM_{00} mode (green). In order to collect only a single TEM_{00} mode, an 8 nm band pass filter (Semrock FF01-690/8-25) is placed in the fluorescence path, and a cavity mode is tuned into this region. Fits yielded N_{sat} values of 495 kcps, 167 kcps and 88 kcps for the full spectrum on the DBR, the full cavity spectrum and a single TEM_{00} mode respectively. Integration of the spectrum shown in figure 3(c) that of the 495 kcps 5.4% of it lies in an 8 nm spectral band centered at 690 nm. This means out of the cavity 26.6 kcps would have been collected through such a filter, in contrast to the 88 kcps measured when the emitter was placed within the cavity. From the ratio of N_{sat} for the cavity-coupled TEM_{00} mode and that of the same NV with only the planar mirror present, we estimate that $\sim$ 17.8% of the emitted fluorescence is output into this single TEM_{00} mode. With a measured TEM_{00} mode width of 0.35 nm this coupling efficiency corresponds to an increase in spectral density by about a factor of 30.

Figure 4 (b) follows the same colour scheme as figure 4(a) and shows measured continuous wave $g^{(2)}(\tau)$ datasets for each case. The degree of photon antibunching observed in $g^{(2)}(0)$ gives an indication of single photon purity. A variety of excitation powers were used; $0.1P_{sat}$(= 0.15 mW), $1.5P_{sat}$(= 0.8 mW) and $2P_{sat}$(= 1.1 mW) for the DBR facing the objective, the full cavity spectrum, and the single TEM_{00} mode datasets. The lower count rates observed for the full cavity and TEM_{00} meant a shift to higher powers facilitated data acquisition. The DBR and full cavity

Optics EXPRESS

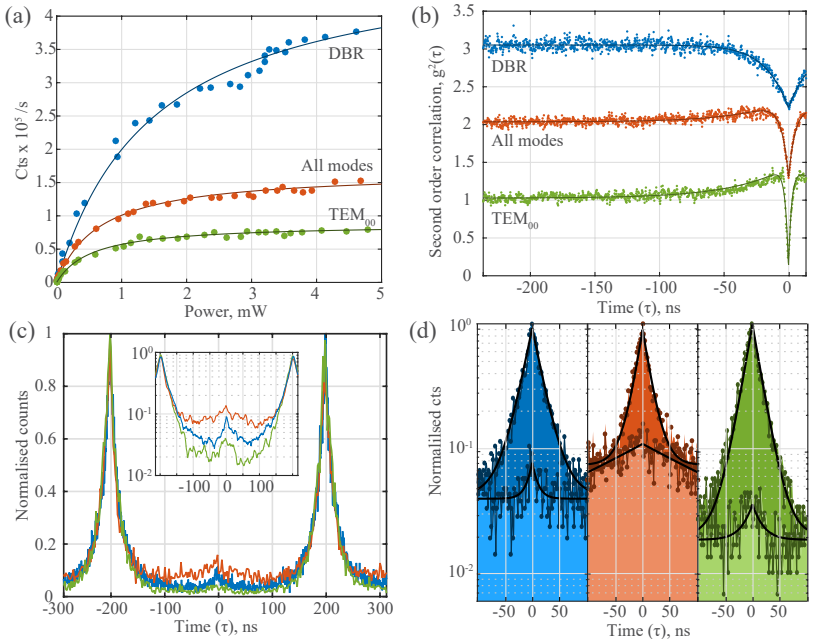

Fig. 4. (a) Saturation curves obtained for NV2 on the DBR facing the collection objective (blue), the full emission when coupled to an RoC 8 μm feature (red), filtered TEM_{00} mode (green). (b) CW HBT measurements performed for the same three situations, showing single photon emission is maintained throughout. The datasets are offset along the y-axis at increments of one unit for clarity. (c) Pulsed HBT measurements for the three situations. The inset highlights a small degradation in single photon purity for the full cavity emission (red), but an improvement when a single mode is filtered (green). (d) Exponential decays with uncorrelated background components are fitted to all three data sets for the regions around $t = 0$ and the peaks at $t = 200$ ns. The colour scheme is maintained (DBR facing objective, all cavity modes and single TEM_{00} mode shown in blue, red and green respectively).

histograms show very similar $g^{(2)}(0)$ values, while the TEM_{00} histogram shows a noticeable reduction in $g^{(2)}(0)$, despite the higher excitation power, as a result of the blocking of broadband background by the bandpass filter.

Quantitative values for device parameters such as the single photon fidelity (ν) and efficiency (η) require pulsed excitation. The laser pulse repetition rate was set to 5 MHz to ensure full decay of the fluorescence between excitation pulses. HBT data to establish the single photon fidelity are shown in figure 4(c) and (d), maintaining the same colour scheme as used in figures 4(a) and (b). The inset shows the central region plotted on a logarithmic scale, with a Gaussian filter applied to remove noise. As with the cw measurements, we find that the presence of the cavity degrades the single photon fidelity if the full spectrum is collected, but the use of a narrow (8 nm) bandpass filter around the TEM_{00} mode restores the fidelity and even improves it compared with that observed in the absence of the cavity. The fact that such strong spectral filtering improves the situation shows that background, uncorrelated light diminishes single photon purity in this system. By using a microcavity to concentrate the NV emission spectrally to a TEM_{00} mode, the benefits of such filtering can be gained without a significant loss in single photon count rate.

Figure 4(d) shows semi-logarithmic plots of curve fits used to quantify the single photon purity in each case. The fitting function comprises rising and falling exponentials, centred at the peak location, upon a time-independent background. This function is fitted to the central peak at $\tau = 0$ and the peak at $\tau = 200$ ns for each measurement.

Optics EXPRESS

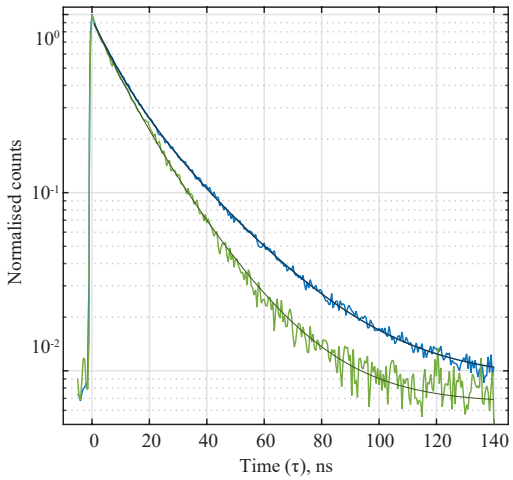

Fig. 5. Time resolved photo luminescence measurements performed on NV2 whilst coupled to an RoC 8 μm cavity (green) and on a DBR facing the objective lens (blue).

The simple ratio of the peak heights reveals the highest purity one could achieve with this device if time gating is included and the uncorrelated background cannot be removed. For the three situations recorded (DBR, full cavity spectrum, TEM_{00} only) we obtain values of ν = 92.7%, 89.1% and 96.3% respectively. The background values provided by the fits for the three situations are 0.041, 0.078 and 0.019 respectively, suggesting that if the uncorrelated signal can be removed fidelities of ν = 96.8%, 96.9% and 98.2% would be achieved.

The device efficiency is estimated by dividing the fitted value of I_{sat} under pulsed illumination by the pulsed excitation rate. This parameter was only measured using the full cavity-coupled spectrum (i.e. with no spectral filter to isolate the TEM_{00}). With the pulsed illumination set at 5 MHz we record I_{sat} = 51 kcps, corresponding to a system efficiency of just over 1%. Using the measured ratio of I_{sat} for the full cavity spectrum to the filtered TEM_{00} under cw excitation, we infer a system efficiency for TEM_{00} mode of $\sim$ 0.5%. Subsequent experiments using planar mirrors with peak reflectivities of 97.5% rather than 99.7% have recorded TEM_{00} mode I_{sat} values of 45 kcps under the same excitation conditions, providing a system efficiency of 0.9%. Taking into account transmission losses in the microscope optics (excluding the objective lens) and the finite efficiency of the single photon detectors we estimate that this corresponds to a device efficiency approaching 3%.

Finally we obtain a further measure of the cavity coupling by comparing the fluorescence lifetime of an NV centre in and out of the cavity. Figure 5 shows time-resolved photoluminescence measurements taken on NV2 when on the DBR substrate facing the mirror (blue) and when cavity coupled (green). Such measurements are insensitive to filtering of the emission and so the full cavity coupled spectrum was used. This plot shows that cavity coupling leads to a marked decrease in the fluorescence lifetime. For both of these decays, the best fits were given by bi-exponential expressions, with a slightly weaker short time component (τ_1) and a longer dominant contribution (τ_2). Whilst the shorter component increased from τ_1 = 7.7 ns to τ_1 = 8.9 ns the dominant part of the decay was seen to decrease from a lifetime of τ_2 = 23.6 ns to τ_2 = 18.6 ns, corresponding to a rate enhancement of 26.3%. The weaker component is a factor of 0.9 smaller than the longer component, which drops to 0.8 when placed inside the cavity. From these results it is not clear what the physical origins of decay route responsible for the shorter lifetime are. The longer decay time is close to the value expected for negatively charged NV centres in nanodiamond.

FDTD simulations reveal a mode volume of $4\lambda^3$, and the effective Q factor of the system is

Optics EXPRESS

shown from $\frac{1}{Q_{eff}} = \frac{1}{Q_{cav}} + \frac{1}{Q_{emit}} = \frac{0.35}{690} + \frac{70}{690}$ to be ≈ 10. From the usual expression for the Purcell factor, $F_p = \frac{3Q_{eff}}{4\pi^2 V}\left(\frac{\lambda}{n}\right)^3$, taking the refractive index of the mode to be 1 corresponding to the air intracavity medium gives $F_P = 0.2$ for the TEM_{00} mode alone, and including proportionate contributions from the other transverse modes present in the measured spectrum in figure 2a gives an effective Purcell factor of 0.3, in excellent agreement with the measured value, once the emission into non cavity modes is taken into account by adding 1. The efficiency of coupling into the TEM_{00} mode of $\beta = F_P/(F_P + 1) = 0.17$, also in excellent agreement with the coupling efficiency measured from the comparison between the measured fluorescence intensities described earlier.

4. Conclusions and outlook

In summary we have reported progress in the realisation of robust, room temperature triggered single photon sources based on the coupling of a single NV centre in nanodiamond to open access microcavities with dielectric mirrors. We have demonstrated optimisation of the cavity parameters by the repeatable coupling of the same single NV centre to a series of engineered cavity mirrors. We find that up to 17% of the room temperature emission is coupled into a single TEM_{00} mode of width 0.35 nm, corresponding to an increase in spectral density by a factor of 30 and demonstrating the important role that cavity feeding in the bad emitter regime can play in achieving a tunable room temperature single photon source. Single photon fidelity in excess of 96% is recorded, along with a recorded single photon device efficiency of around 3%. Such device specifications hold promise for the realisation of practical triggered single photon sources operating at room temperature.

Funding

European Commission (FP7 WASPS), grant agreement number 618078.

Acknowledgments

S.A. and S. J. acknowledge support from the UK Engineering and Physical Sciences Research Council. A.A.P.T. and L.F. acknowledge support from the Leverhulme Trust.